Scientia Iranica F (2017) 24(6), 3481–3490

Sharif University of Technology
Scientia Iranica
Transactions F: Nanotechnology
www.scientiairanica.com

Investigation of carbon phase evolutions in titanium nitride-carbon nanocomposites prepared in supercritical benzene with respect to their lithium storage capacity

E. Yousefi[a,b,*], M. Ghorbani[a,*], A. Dolati[a] and H. Yashiro[b]

a. *Department of Materials Science and Engineering, Sharif University of Technology, Tehran, P.O. Box 11155-9466, Iran.*
b. *Department of Chemistry and Bioengineering, Faculty of Engineering, Iwate University, 4-3-5 Ueda, Morioka, Iwate 020-8551, Japan.*

Received 8 August 2016; accepted 29 October 2016

KEYWORDS
Titanium nitride-graphene nanocomposite;
Carbon phase evolution;
Supercritical benzene;
Li ion battery.

Abstract. Titanium nitride-carbon nanocomposites have been synthesized by the reaction of $TiCl_4$ and NaN_3 in supercritical benzene medium that also serves as a carbon source. The as-prepared precursor has been subjected to different heat treatments under ammonia and nitrogen atmospheres. The structure and chemical composition of the synthesized TiN-C nanocomposites are studied by X-Ray Diffraction (XRD) and CHN elemental analysis. Meanwhile, the nature of carbonaceous species and the respective carbon phase transitions during supercritical process and following heat treatments are further investigated by Raman spectroscopy, Time of Flight Secondary Ion Mass Spectrometry (ToF-SIMS), and their charge-discharge characteristics with respect to lithium storage. After 10 h of NH_3 treatment at 1000°C, carbonaceous phase transforms to graphene layered structure. The highly efficient mixed TiN conducting network and the internal defects between G layers induced by nitrogen doping improve rate capability and cycling performance of G sheets and provide a specific capacity of 381 mAh g^{-1} at Charge/Discharge (C/D) rate of 0.2 C. The enhanced electrochemical performance of the SIV nanocomposite is mainly due to improving the electronic/ionic conductivity, reducing charge transfer coefficient, and increasing electrochemical surface area that are resulted from anchoring of TiN nanoparticles to graphene sheets.

1. Introduction

Lithium Ion Batteries (LIBs) with high energy density, long cycle life, and environmentally friendly aspect are important power sources in portable electronics and electric vehicles. Layered structure carbonaceous materials are widely used as anodes in commercial LIBs because of their good specific capacity and low cost [1]. However, their poor rate capability and cycling performance, because of failure of carbon structure, cannot meet the upward requirements for high-performance LIBs [2,3]. Recently, there have been tremendous efforts to improve carbonaceous anodes performance by doping various elements as conducting agent or decreasing crystallite size and increasing pore structure [3,4]. Using active-inactive composites as a mixed-conductive matrix, which electrically isolates the active particles from the current collector, is one of the solutions to improve the anode performance. The inactive

*. *Corresponding authors. Tel.: +98 21 6616 5219; Fax: +98 21 66005717*
E-mail addresses: yousefi@mehr.sharif (E. Yousefi); ghorbani@sharif.edu (M. Ghorbani); dolati@sharif.edu (A. Dolati); yashiro@iwate-u.ac.jp (H. Yashiro)

doi: 10.24200/sci.2017.4417

Table 1. Synthesis and heat treatment conditions.

Sample	Synthesis conditions		Heat treatment		
	Temperature (°C)	Time (h)	Atmosphere	Temperature (°C)	Time (h)
SI	380	1	—	—	—
SII	380	8	—	—	—
SIII	380	1	NH_3	1000	3
SIV	380	1	NH_3	1000	10
SV	380	1	N_2	1000	10

phase can avoid aggregation of the particles and recover electrical connection between the anode particles and the current collector [5,6]. Titanium nitride (TiN) shows excellent chemical resistance, superior electrical conductivity, and good adhesion with most materials. Therefore, there are great interests in upgrading anode performance by doping TiN into anode matrix. Anchoring of TiN nanoparticles to graphene layers not only promotes the electrical conductivity along c-axis, but also suppresses the agglomeration of graphene sheets, resulting in the formation of a flexible porous texture [7-10].

In the present study, TiN-C nanocomposites have been prepared using benzene as a carbon source through partial decomposition under supercritical condition followed by different heat treatments under ammonia and nitrogen atmospheres. However, our previous study has revealed the formation pathway of TiN-C nanocomposites and discussed their oxygen reduction activities [10]. Regarding the importance of carbon crystalline structure and its effect on electrochemical performance, in an attempt to understand the nature of carbonaceous species, the present work is directed towards studying the respective carbon phase transitions. X-Ray Diffraction (XRD), Raman spectroscopy, Time of Flight Secondary Ion Mass Spectrometry (ToF-SIMS), and CHN elemental chemical analyses are used to identify the structure and nature of the carbonaceous species in the synthesized nanocomposites. Moreover, to confirm the obtained results, the specific capacities of the prepared nanocomposites are measured as an anode in LIBs. In the active-inactive composite of C and TiN, C acts as a reactant during the lithiation process to form Li_xC, which is enclosed by the TiN inactive matrix. Since Li^+ can only intercalate into carbon layered structures, and considering the theoretical specific capacity of graphite as 372 mAh g^{-1}, the specific capacity of synthesized anodes can be a representative of their structure. The TiN in the composite electrode does not alloy with lithium, but serves as an inactive matrix to support the intergrain electronic contact in the material, which would enable the TiN-C nanocomposite to exhibit good rate capability and cycling performance.

2. Experimental

2.1. TiN-C nanocomposites synthesis

TiN-C nanocomposites were synthesized by a supercritical process using benzene (C_6H_6, Merck, 99.96%) as a solvent and carbon source and titanium tetrachloride ($TiCl_4$, Merck, $>$ 99%) and sodium azide (NaN_3, Merck, $>$ 99%) as reactants at 380°C with the holding time of 1-8 h. Subsequently, the as-prepared sample (SI) was further heat treated at 1000°C for 3-10 h using NH_3 and N_2 atmospheres, as mentioned in Table 1.

2.2. Characterization

In order to examine the phase evolution and crystallization behavior, a STOE D-64295 diffractometer (Cu-Kα radiation, $\lambda = 1.54056$Å) was used employing a step size of 0.015. To evaluate the structural parameters of microcrystalite diameter (L_a) and interlayer spacing (L_c) for carbonaceous structure, XRD patterns were analyzed using the classical Debye-Scherer equations [11]:

$$L_c = 0.90\lambda/\beta_{002}\cos\theta_{002}, \quad (1)$$

$$L_a = 1.94\lambda/\beta_{100/101}\cos\theta_{100/101}, \quad (2)$$

where β stands for Full Width at Half Maximum (FWHM) in radians of θ.

In order to evaluate the nature of the crystalline structure of the carbonaceous species and the order/disorder degree of layered structure in the prepared samples, Raman spectra were taken on an ALMEGA XR Raman spectrometer at 532 nm. The intensity, position, and width of the bands were obtained using a Gaussian curve fitting procedure. The microcrystalline diameter (L_a) in amorphous carbons can be calculated by the following equation [12]:

$$C(\lambda)L_a^2 = \left(\frac{I_D}{I_G}\right), \quad (3)$$

where $C(\lambda)$ is given to be ~ 0.0055 for $\lambda = 514$ nm, which can be assumed as comparable with our slightly different λ (532 nm) [13]. Meanwhile, the crystallite size (L_a) of graphene structure can be calculated by Tuinstra and Koening (TK) equation as mentioned below:

$$L_a = (2.4 \times 10^{-10})\lambda_{\text{laser}}^4 \left(\frac{I_D}{I_G}\right)^{-1}, \quad (4)$$

where λ_{laser} denotes laser line wavelength in nm units. Moreover, to have better an insight into molecular reactions during supercritical process and subsequent heat treatments, ToF-SIMS analysis was carried out on the synthesized samples to study the surface chemicals with a TRIFT V, ULVAC-PHI Inc. time-of-flight secondary ion mass spectrometer equipped with a Bi liquid-metal cluster ion source. Positive and negative ion spectra were acquired with a pulsed, electrodynamically compressed 30 keV primary ion beam by railing the ion beam over a 16.4 μm × 16.4 μm sample area. The primary ion dose was kept below 4.7×10^{13} ions/cm^2 to maintain static SIMS conditions. The results were analyzed with "WinCadence N" software. The peaks were normalized to $^{48}Ti^+$ and CN^- peak intensities for positive and negative spectra, respectively, to correct differences in the total secondary ion yield from spectrum to spectrum, as a result of instrumental drift, and provide better comparison state between different spectra. The prepared nanocomposites were also analyzed chemically using a Yanaco CHN CORDER MT-6 carbon, hydrogen, and nitrogen analyzer to determine the amount of carbon in the samples.

2.3. Electrochemical measurements

The electrochemical properties of the synthesized samples were examined using a two-electrode electrochemical cell at room temperature. The working electrodes were prepared by mixing active material, and poly(vinylidene difluoride) (PVDF) binder in a weight ratio of 95:5 without adding any conductive material in NMP solvent to form a homogeneous slurry and pasted on a copper foil, and then dried in vacuum oven at 80°C for 12 h. Lithium foil was used as the counter electrode and was separated from the anode by a Celgard® 2400 membrane. The electrolyte was 1.0 M $LiPF_6$ in a mixture of Ethylene Carbonate (EC), dimethyl carbonate (DMC), and diethyl carbonate (DEC) with a volumetric ratio of 1:1:1. The cells were charged and discharged over a voltage range of 0.005-3.0 V (versus Li/Li^+) at 0.2 C-rate using a charge-discharge unit (Hokuto Denko, HJ-1010 M) in a galvanostatic mode. Electrochemical Impedance Spectroscopy (EIS) measurements were performed using a potentionstat Ivium CompactStat by applying an AC voltage of 10 mV amplitude in the frequency range of 10 mHz-100 kHz at room temperature.

3. Results and discussion

3.1. Characterization

Figure 1 shows the XRD spectra of the powders heat treated under different conditions as mentioned in Table 1. The as-prepared sample (SI) demonstrates the presence of TiN crystalline phase with characteristic peaks of 36.8°, 42.6°, 62.0°, and 74.2° accompanied with carbonaceous structure. The wide (002) peak between 12-32° can be deconvoluted into two peaks (Figure 1(b)-(e)), implying the existence of carbon species in turbostratic or random layer lattice structure [14]. With increasing resident time (SII), the related peak intensities, crystallite size, carbon content, and benzene decomposition into aliphatic chains raise. After 3 h of NH_3 treatment, TiN diffraction peaks' intensities ascend sharply; consequently, the crystallite size increases from 15 nm up to 38 nm. Moreover, the peaks' positions of carbonaceous species slightly shift to smaller values that indicate the phase transformation to graphene layered structure. Although further NH_3 treating does not have any significant effect on TiN crystallization or crystallite size, carbon crystallization continues and microcrystalline diameter and interlayer spacing increase from 74 nm up to 99 nm and 9.23 Å up to 10.90 Å, respectively. However, after 10 h of N_2 treatment (SV) at 1000°C, XRD pattern indicates the presence of β-TiO_2 with monoclinic structure and carbon peaks related to graphite structure.

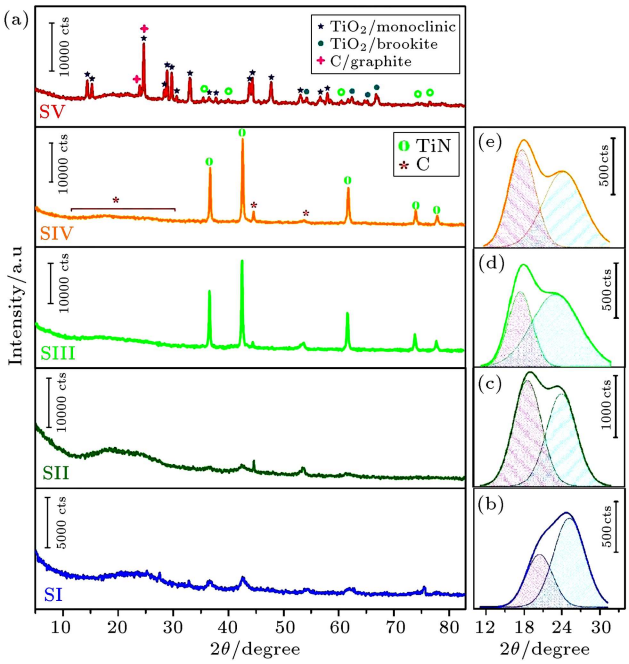

Figure 1. (a) X-ray diffraction patterns of different samples according to Table 1 and related carbon peak deconvolutions for (b) SI, (c) SII, (d) SIII, and (e) SIV samples.

Figure 2 shows Raman spectra of SI-SV samples and their appropriate peak deconvolution. Samples SI and SII show peaks centered at 1604, 1543, 1333, and 1231 cm^{-1} that are attributed to G, amorphous carbon, D, and sp^3 rich phase, respectively [15,16]. The presence of wide peak at around 3000 cm^{-1} is

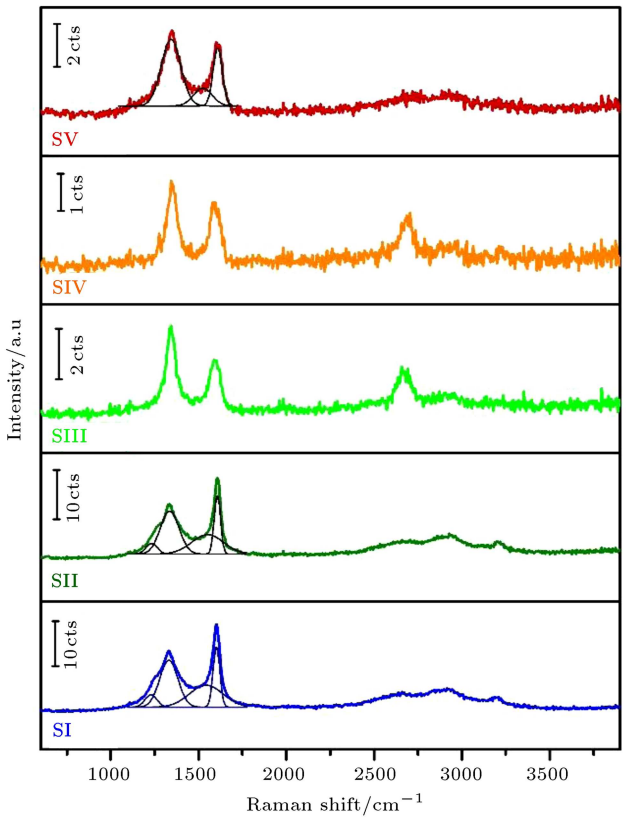

Figure 2. Raman spectra of SI-SV samples and their deconvoluted peaks.

due to amorphous carbon while small peaks at 3189, 2914, and 2658 cm^{-1} are assigned to 2G, D+G, and 2D peaks. Regarding the literature, the presence of D, G, 2D, D+G, and 2G peaks reveals the presence of damaged graphene structure. On the other hand, the high intensity of G and D peaks indicates dispersed graphene layers in an amorphous carbon matrix, while wide D peak shows the ring order other than six for ringed sp^2 carbon [12,17]. These data and analyses determine the carbonaceous phase structure in the as-prepared samples as turbostratic or random layered lattice with I(D)/I(G) ratio and graphene crystallite size of 0.79 and ∼11 nm, respectively. After 3 h of NH_3 treatment, the carbon phase transforms totally to sp^2 state and graphene structure. The presence of G peak demonstrates E_{2g} mode of graphite, which is related to the vibration of sp^2 bonded carbon atoms in a 2-dimensional hexagonal lattice. Meanwhile, the presence of D peak is an indication of defects associated with vacancies, grain boundaries, and amorphous carbon species [18]. Moreover, the presence of 2D peak is the evidence of bi-layer graphene structure and good indication of c axis ordering. Raman spectra with characteristic G and D bands are implications of defects, disorder, and carbon grain size; their intensity ratio (I(D)/I(G)) is related to the level of disorder degree and average size of sp^2 domains [12,19]. In this case, the graphene crystallite size can be calculated using Eq. (4) and I(D)/I(G) = 1.68 as ∼11 nm. Further heat treatment leads to ring opening of sp^2 atoms and subsequent decreasing of I(D)/I(G) ratio and increases the order degree of graphene layers. Therefore, more atoms are placed in sp^2 chains, and graphene crystallite size increases to ∼16 nm. The observed differences between L_a estimated by TK and Debye-Scherer equations can be related to the possibility that XRD spectrum weights are the bigger crystallites, while TK underestimates L_a due to the dominant effect of small crystallites [12]. Thus, it can be concluded that the microcrystallite diameter of graphene patches of SIV is between 16-99 nm.

However, heat treating under inert atmosphere leads to different structures with peaks at 1608, 1541, and 1344 cm^{-1}. Considering the weak peak centered at 2833 cm^{-1} and its deconvolution, it can be concluded that SV consists of hexagonal graphitic structure with crystallite size of ∼17 nm. Besides, it seems that there is still some untransformed amorphous carbons in the SV sample after 10 h of N_2 treatment. This evidence shows the effect of reactive atmosphere on not only complement of TiN nitridation, but also on carbon phase evolution. The main reason for this is that, under ammonia atmosphere, the phase transition temperature of carbonaceous species reduces to 800°C, while, in N_2 atmosphere, this temperature will be as high as 1500°C [20,21]. Moreover, under N_2 atmosphere, the presence of carbonaceous species prevents the crystallization and growth of the TiN crystals during heat treatment [22].

To have more understanding on the supercritical process reactions and the following heat treatment mechanism, the chemical state of the synthesized powders was investigated by positive/negative ion ToF-SIMS analysis. Figure 3 represents positive ToF-SIMS spectra of different samples with the most intense peak of $^{48}Ti^+$ at m/z of 47.95 u. All Ti isotopes are also seen in the ToF-SIMS patterns. Moreover, the peaks at 61.95, 63.94, and 64.95 assigned to $^{48}TiN^+$, $^{48}TiO^+$, and $^{48}TiOH^+$ ion fragments, respectively, are significantly intense as well. Meanwhile, the isotopes of these compounds experience some overlaps. The peaks at 59.96 and 60.96 are assigned to $^{46}TiN^+$ and $^{47}TiN^+$ ion fragments, respectively. Meanwhile, the peak at 61.95 relates to $^{48}TiN^+$ and $^{46}TiO^+$ fragments. The peak at 62.96 corresponds to $^{49}TiN^+$, $^{47}TiO^+$, and $^{46}TiOH^+$. Further, the peak at 63.95 relates to $^{50}TiN^+$, $^{48}TiO^+$, and $^{47}TiOH^+$. The peak at 64.95 stands for $^{49}TiO^+$ and $^{48}TiOH^+$ and the peak at 65.96 reveals $^{50}TiO^+$ and $^{49}TiOH^+$. Moreover, the peak at 66.96 assigns to $^{50}TiOH^+$ ion fragment. The relative intensity of each compound in the overlapped peaks can be calculated based on Ti isotopes distribution. The presence of oxygen, which is always detected, is due to

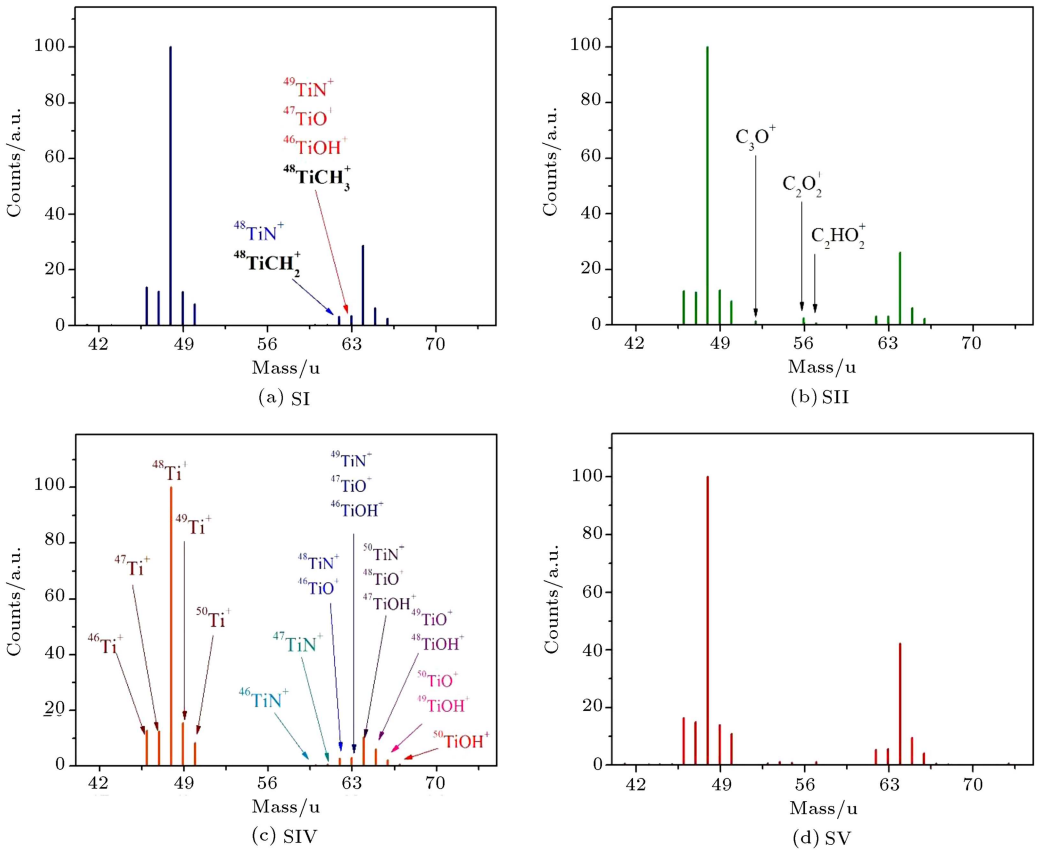

Figure 3. Positive ion ToF-SIMS spectra of the synthesized TiN-C nanocomposites by different conditions: (a) SI, (b) SII, (c) SIV, and (d) SV.

moisture or oxygen uptake during air exposure after the synthesis process and/or oxygen or water released from the water in the washing step. The remaining amount of Ti-O bonds which are in amorphous state according to XRD patterns is unavoidable due to partial surface oxidation of TiN compounds after heat treatment. The characteristic peaks of the analyzed precursor and their assignments are demonstrated in Figure 3. By comparing the positive ion spectra of the precursors synthesized for 1 (SI) and 8 h (SII), increasing resident time mostly leads to formation of carbide species and increasing relative intensity of some other compounds such as CHN, C_2O_2, and HNO_2. However, the benzene molecular ion (i.e., C_6H_5Ti expected at 124.99 m/z) was not detected, but the presence of some organic compounds on the surface of the precursor would attest to benzene partial decomposition under supercritical condition and subsequent reacting with azide groups and formation of C-H, C-H-N or C_2H_4N bonds on the surface of the precursor. According to this observation, benzene decomposition and its reaction with azide groups and titanium tetrachloride would be increased with rising holding time. It is worth mentioning that some compounds, such as $TiCH_3$, in the ToF-SIMS spectra of the as-prepared precursor with weak peak intensity are detected which represent the benzene circles broken and that consequent hydrocarbons react with $TiCl_4$. The ToF-SIMS data indicate some organic functional groups existing on the surface of the precursor.

After applying heat treatment, almost all functional groups, such as C-H bands and NO_2 groups, on the surface of as-prepared precursor are removed. Moreover, it can be seen that, after heat treatment, the relative peak intensities of TiO, TiOH, and $TiCH_x$ bonds decrease. The remaining amount of oxide bonds is unavoidable due to partial surface oxidizing of TiN compounds. As well, SIMS data do not expose any other important difference between chemical composition of NH_3 treated samples for 3 h and 10 h. However, SV shows more intense TiO peak, in addition to some small peaks that are assigned to oxynitride/carbonitride species.

To have a better understanding on the carbon ion species and phase evolutions, the negative ToF-SIMS spectra of SI and SIV samples and the related peak assignments are shown in Figure 4. Carbon bonding states are present in sp^2 and sp^3 of C^-, C_2^-, C_3^-, C_4^-, and C_6^- at m/z of 12.00, 24.00, 36.00, 48.00, and 72.00 u, respectively, while the highest intensity results from C_2^-. The presence of CN^- ion mass fragment in the SI reveals the incorporation of N into carbon

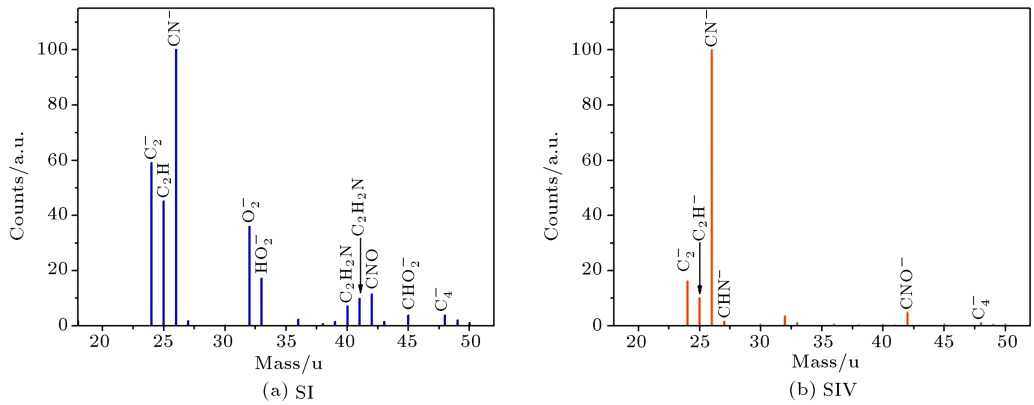

Figure 4. Negative ion ToF-SIMS spectra of the synthesized TiN-C nanocomposites by different conditions: (a) SI and (b) SIV.

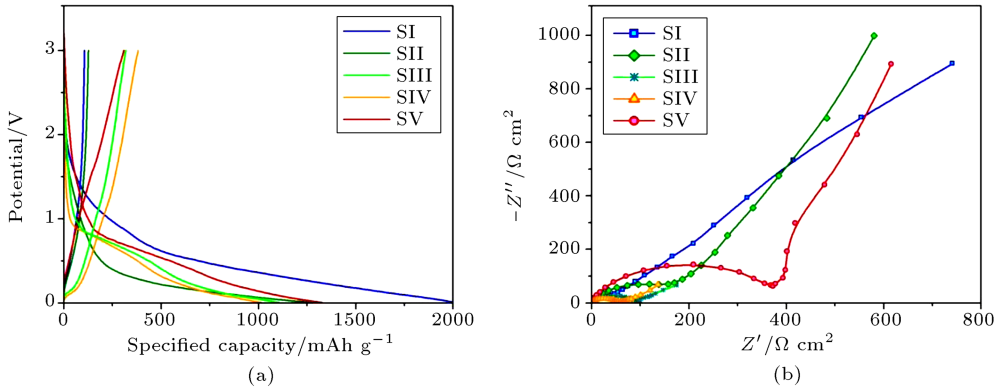

Figure 5. Electrochemical performance of the synthesized samples as anode in 1 M $LiPF_6$-EC:DMC:DEC (vol. 1:1:1) electrolyte: (a) First C/D curves cycled at 0.2 C between 3 and 0.005 V vs. Li/Li^+, and (b) Nyquist plots at 3.0 V vs. Li/Li^+ before cycling.

lattice, meaning that azide groups are a nitrogen source for both Ti and carbon atoms. After 10 h of NH_3 treating at 1000°C, the peak intensity of CN^- ion fragment increases around 6 times. The doped nitrogen would affect the graphene properties and performance. At first, it would disrupt sp^2 hybridization of carbon atoms and affect electronic properties [23]. Moreover, it would enhance carrier density and, consequently, increase the conductivity of graphene [24]. Finally, it would remarkably increase the graphene specific capacitance [25]. The presence of some CH and CHN compounds in the negative SIMS spectra of SIV can be attributed to the presence of saturated structures, such aliphatic side chains, attached to the edge of the carbon crystallites.

To have a more accurate comprehension on the chemical composition of the synthesized TiN-C nanocomposites, and specially provide a quantitative measure of the carbon contain, CHN analysis was conducted and the results are shown in Table 2.

3.2. Electrochemical performance

To determine the electrochemical performances of the synthesized TiN-C nanocomposites as anodes in LIB,

Table 2. Elemental analysis of various samples prepared in different conditions.

Sample	C (wt%)	H (wt%)	N (wt%)
SI	41.66	2.28	2.51
SII	50.12	2.37	3.10
SIII	44.08	1.40	10.06
SIV	35.99	0.67	10.78
SV	16.89	0.42	1.26

galvanostatic C/D cycles have been performed at a rate of 0.2 C over a potential range of 0.005-3.0 V (versus Li/Li^+), shown in Figure 5(a). The calculated specific capacities are obtained based on C mass as active material. The synthesized samples SI, SII, SIII, SIV, and SV demonstrate specific capacity of 105, 125, 317, 381, and 307 mAh g^{-1} with columbic efficiency of 5, 10, 29, 38, and 23%, respectively. These results confirm the characterization analysis and show the existence of random layered structure in the as-prepared samples. The specific capacities of SI and SII samples that are 0.28 and 0.34 of theoretical specific capacity of graphite structure, respectively, reveal that the carbon has a random layered structure in these nanocomposites

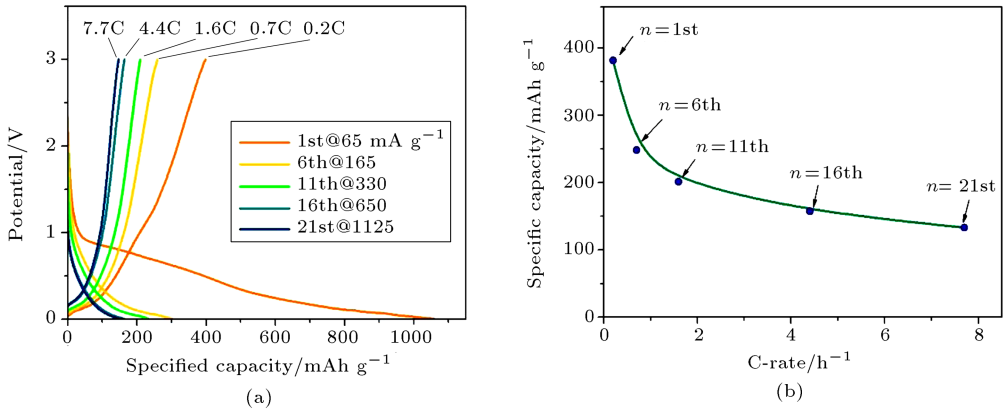

Figure 6. Electrochemical performance of the TiN/G nanocomposite as anode in 1 M $LiPF_6$-EC:DMC:DEC (vol. 1:1:1) electrolyte cycled between 3 and 0.005 V vs. Li/Li^+: (a) C/D curves cycled with different rates as n = 1st∼5th @ 0.2 C, n = 6th∼10th @ 0.7 C, n = 11th∼15th @ 1.6 C, n = 16th∼20 @ 4.4 C, and n = 21st∼25 @7.7 C-rate, and (b) the specific capacity as a function of C/D rate.

that is in accordance with XRD and Raman analysis. Moreover, increasing resident time not only leads to more benzene decomposition, but also helps for more carbon crystallization. Increasing NH_3 treating time leads to ordering graphene structure and, consequently, improving electrochemical performance of SIV compare with SIII. The specific capacity of SV sample is 0.83 of theoretical specific capacity of graphite structure that confirms the existence of an amorphous phase with graphite structure. It is apparent that all TiN-C nanocomposites showing a huge irreversible capacity loss on the first cycle can be attributed to: (1) the incapability of removing all the lithium on discharge that is inserted onto the first charge; (2) the reduction of the electrolyte on the electrode surface and formation of Solid Electrolyte Interface (SEI) [26-29]. Li ions can be trapped into graphene defect sites because of reacting with surface functional groups [30-32]. The EIS measurements that have been done before cycling at 3.0 V versus Li/Li^+ and the corresponding Nyquist plots are shown in Figure 5(b), indicating that the impedance of samples reduces with the application of heat treatment because of crystallization of both TiN and C phases. Moreover, TiN nanoparticles increase conductivity of SIV and, consequently, lead to the decrease of the impedance compared with SV sample. These results show that anchoring of TiN nanoparticles on G sheets enhances the electrochemical performance by improving the electronic/ionic conductivity, reducing charge transfer coefficient, and increasing electrochemical surface area. Based on these analyses, under supercritical condition with temperature as low as 380 °C and pressure around 150 atm., the carbonaceous phase with random layered structure is achievable. After applying NH_3 treating, the carbon phase transforms into graphene-layered structure. Meanwhile, increasing heat treatment time, mostly, leads to growing up and ordering of graphene layers.

Considering the notable specific capacity of SIV, its electrochemical performance is further investigated. In this regard, galvanostatic C/D cycles have been performed at different rates (Figure 6(a)), and the corresponding relationship between the specific capacities and the current densities acquired from the C/D curves in Figure 6(a) are depicted in Figure 6(b). The TiN/G nanocomposite conveys a specific capacity of 381 mAh g^{-1} at a current density of 0.2 C. Meanwhile, at higher current density of 7.7 C, a remarkable specific capacity of 133 mAh g^{-1} is also delivered that represents a good rate capability. It is worth noting that the specific capacity of G in TiN/G nanocomposites increases as a function of G in proportion up to 641 mAh g^{-1} at 65% G [7,8]. Afterwards, the extra addition of G leads to decreasing the specific capacity of G to 218 mAh g^{-1} at 82% G with C/D rate of 0.5 C, which is almost equal to G performance. The synthesized TiN/G nanocomposite with 36% G and a specific capacity of 254 mAh g^{-1} are in accordance with the provided trend that suggests comparable quality of G sheets. The decrease of specific capacity in low content TiN composites may ascribe to the insufficient cover of TiN on G that leads to producing large amount of SEI on the surface of electrode. Meanwhile, the decrease of specific capacity in composites with high amounts of TiN is due to the excess inactive TiN that reduces the reversible capacitance. Using supercritical process to fabricate TiN/G nanocomposite, the percentage of G that is a function of benzene decomposition can be controlled by process time [10] and temperature [33].

According to differential capacity analysis, as depicted in Figure 7, there are different Li storage sites in the synthesized TiN/G anode that could be divided into three areas, namely below 0.5, between 0.5-1.3, and above 1.3 V versus Li/Li^+. Three pairs of reversible peaks below 0.5 V versus Li/Li^+ are due to lithium insertion into the graphene layers [34,35].

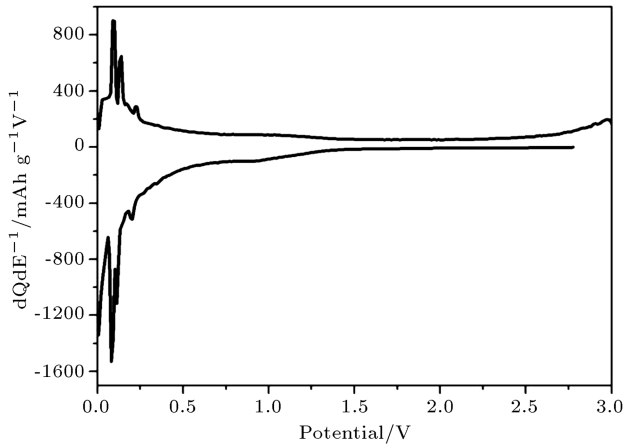

Figure 7. Derivative dx/dV plotted vs. voltage of the 30th cycle of TiN/G electrode cycled between 3 and 0.005 V vs. Li/Li$^+$ at C/25.

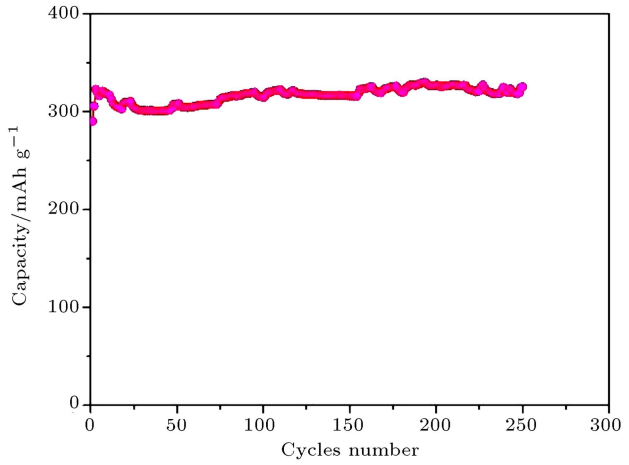

Figure 8. Cycling performance at 1.6 C-rate using TiN/G electrode as an anode material.

On the other hand, between 0.5-1.3 V versus Li/Li$^+$, lithium ions are intercalated into micropores, while double-layer mechanism is the prominent phenomenon at higher potentials.

The TiN/G demonstrates good cycling behavior as indicated in Figure 8. At first, specific capacity initially increases up to 1.1 times during the first three cycles that can be attributed to the boosting of its porous network structure. During Li insertion and extraction process, in the initial cycles, the TiN clusters pulverize into small particles due to electrochemical milling effects that lead to more porous nanostructures with more edges, which are able to provide more activated sites for Li storage and also facilitate the penetration of the electrolytes [18,36]. Establishing diffusive condition because of SEI formation leads to a capacity retention (C15/C3) of 95%. Afterwards, the capacity starts to ascend due to gradual extraction of trapped Li ions into SEI or cavities [37] in such a way that shows capacity retention of 112% after 250 cycles. Actually, it seems that the larger number of lithiation/delithiation cycles activates electrochemical processes associated to the diffusion of Li$^+$ that allows the trapped Li$^+$ to be gradually extracted from the micropores, and so the capacity increases.

4. Conclusion

TiN-C nanoparticles were synthesized using $TiCl_4$ and NaN_3 reactants in supercritical benzene medium that also serves as a carbon source and, afterward, applies heat treatment under NH_3 and N_2 atmospheres. The evolutions of carbon phase during supercritical process and following heat treatments were studied extensively. After 10 h of NH_3 treating at 1000°C, amorphous carbon was transferred to N-doped graphene structure, while N_2 treating led to a different structure. The synthesized nanoparticles were tested as anodes for LIBs. The TiN/G material exhibited superior electrochemical performance as an anode for LIBs with specific capacities of 381 and 133 mAh g^{-1} at C/D rates of 0.2 and 7.7 C, respectively. Meanwhile, TiN/G electrode depicts the capacity retention of 99% after 250 cycles at C/D rate of 0.7 C. The favorable electrochemical performance of TiN/G anode is related to the highly efficient mixed conducting network and doping nitrogen into graphene sheets, improving the electronic/ionic conductivity, reducing charge transfer coefficient, and increasing electrochemical surface area. The introduced facile synthesis of TiN/G nanocomposite provides an advantageous pathway towards the development of high energy density, long cycle life, and commercial Li-ion anodes by anchoring of TiN nanoparticles to G that promotes energy storage applications in high-performance lithium-ion batteries.

Acknowledgement

The authors are grateful for the partial financial support of this study by research council of Sharif University of Technology. Moreover, authors would like to thank Ms. M. Watanabe for worthwhile helps about ToF-SIMS experiments.

References

1. Pan, D., Wang, S., Zhao, B., Wu, M., Zhang, H., Wang, Y. and Jiao, Z. "Li storage properties of disordered graphene nanosheets", *Chem. Mater.*, **21**(14), pp. 3136-3142 (2009).
2. Xiang, H.F., Li, Z.D., Xie, K., Jiang, J.Z., Chen, J.J., Lian, P.C., Wu, J.S., Yu, Y. and Wang, H.H. "Graphene sheets as anode materials for Li-ion batteries: preparation, structure, electrochemical properties and mechanism for lithium storage", *RSC Adv.*, **2**(17), pp. 6792-6799 (2012).

3. Wang, H., Zhang, C., Liu, Z., Wang, L., Han, P., Xu, H., Zhang, K., Dong, S., Yao, J. and Cui, G. "Nitrogen-doped graphene nanosheets with excellent lithium storage properties", *J. Mater. Chem.*, **21**(14), pp. 5430-5434 (2011).

4. Chen, M.-H., Wu, G.-T., Zhu, G.-M., You, J.-K. and Lin, Z.-G. "Characterization and electrochemical investigation of boron-doped mesocarbon microbead anode materials for lithium ion batteries", *J. Solid State Electrochem.*, **6**(6), pp. 420-427 (2002).

5. Kim, S.-J., Park, H.-C., Kim, M.-C., Kim, D.-M., Lee, Y.-W. and Park, K.-W. "Sputtered amorphous thin film nanocomposites as an anode for lithium-ion batteries", *J. Power Sources*, **273**, pp. 707-715 (2015).

6. Yan, C., Xi, W., Si, W., Deng, J. and Schmidt, O.G. "Highly conductive and strain-released hybrid multilayer Ge/Ti nanomembranes with enhanced lithium-ion-storage capability", *Adv. Mater.*, **25**(4), pp. 539-544 (2013).

7. Yue, Y., Han, P., He, X., Zhang, K., Liu, Z., Zhang, C., Dong, S., Gu, L. and Cui, G. "In situ synthesis of a graphene/titanium nitride hybrid material with highly improved performance for lithium storage", *J. Mater. Chem.*, **22**(11), pp. 4938-4943 (2011).

8. Han, P., Yue, Y., Wang, X., Ma, W., Dong, S., Zhang, K., Zhang, C. and Cui, G. "Graphene nanosheet-titanium nitride nanocomposite for high performance electrochemical capacitors without extra conductive agent addition", *J. Mater. Chem.*, **22**(47), pp. 24918-24923 (2012).

9. Lu, X., Wei, H., Chiu, H.-C., Gauvin, R., Hovington, P., Guerfi, A., Zaghib, K. and Demopoulos, G.P. "Rate-dependent phase transitions in Li_2FeSiO_4 cathode nanocrystals", *Sci. Rep.*, **5**, p. 8599 (2015).

10. Yousefi, E., Ghorbani, M., Dolati, A., Yashiro, H. and Outokesh, M. "Preparation of new titanium nitride-carbon nanocomposites in supercritical benzene and their oxygen reduction activity in alkaline medium", *Electrochim. Acta*, **164**, pp. 114-124 (2015).

11. Sakintuna, B., Yurum, Y. and Cetinkaya, S. "Evolution of carbon microstructures during the pyrolysis of Turkish elbistan lignite in the temperature range 700-1000°C", *Energy Fuels*, **18**(3), pp. 883-888 (2004).

12. Ferrari, A.C. "Raman spectroscopy of graphene and graphite: Disorder, electron-phonon coupling, doping and nonadiabatic effects", *Solid State Commun.*, **143**(1-2), pp. 47-57 (2007).

13. Childres, I., Jauregui, L.A., Park, W., Cao, H. and Chen, Y.P. "Raman spectroscopy of graphene and related materials", In *New Developments in Photon and Materials Research*, Jang, J. I., Ed., pp. 1-20, Nova Science Publishers, New York (2013).

14. Manoj, B. and Kunjomana, A.G. "Study of stacking structure of amorphous carbon by X-ray diffraction technique", *Int. J. Electrochem. Sci.*, **7**, pp. 3127-3134 (2012).

15. Jorio, A., Saito, R., Dresselhaus, G. and Dresselhaus, M.S. "Raman spectroscopy: from graphite to sp^2 nanocarbons", In *Raman Spectroscopy in Graphene Related Systems*, pp. 73-101, Wiley-VCH Verlag GmbH & Co. KGaA (2011).

16. Pimenta, M.A., Dresselhaus, G., Dresselhaus, M.S., Cancado, L.G., Jorio, A. and Saito, R. "Studying disorder in graphite-based systems by Raman spectroscopy", *Phys. Chem. Chem. Phys.*, **9**(11), pp. 1276-1290 (2007).

17. Ferrari, A.C. and Robertson, J. "Raman spectroscopy of amorphous, nanostructured, diamond-like carbon, and nanodiamond", *Phil. Trans. R. Soc. A*, **362**(1824), pp. 2477-2512 (2004).

18. Liu, L., An, M., Yang, P. and Zhang, J. "Superior cycle performance and high reversible capacity of SnO_2/graphene composite as an anode material for lithium-ion batteries", *Sci. Rep.*, **5**, p. 9055 (2015).

19. Tamuleviciene, A., Kopustinskas, V., Niaura, G., Meskinis, S. and Tamulevicius, S. "Multiwave length Raman analysis of SiO_x and N containing amorphous diamond like carbon films", *Thin Solid Films*, **581**, pp. 86-91 (2015).

20. Cui, T., Lv, R., Huang, Z.-H., Zhu, H., Jia, Y., Chen, Sh., Wang, K., Wu, D. and Kang, F. "Low-temperature synthesis of multilayer graphene/amorphous carbon hybrid films and their potential application in solar cells", *Nanoscale Res. Lett.*, **7**, p. 453 (2012).

21. Barreiro, A., Borrnert, F., Avdoshenko, S.M., Rellinghaus, B., Cuniberti, G., Rummeli, M.H. and Vandersypen, L.M.K. "Understanding the catalyst-free transformation of amorphous carbon into graphene by current-induced annealing", *Sci. Rep.*, **3**, p. 1115 (2013).

22. Kim, I.-S. and Kumta, P.N. "Hydrazide sol-gel synthesis of nanostructured titanium nitride: precursor chemistry and phase evolution", *J. Mater. Chem.*, **13**, pp. 2028-2035 (2003).

23. D'Souza, F. and Kadish, K.M., *Handbook of Carbon Nano Materials: (in 2 volumes) Volume 5: Graphene-Fundamental Properties Volume 6: Graphene-Energy and Sensor Applications*, p. 552, World Scientific (2014).

24. Pu, N.-W., Peng, Y.-Y., Wang, P.-C., Chen, C.-Y., Shi, J.-N., Liu, Y.-M., Ger, M.-D. and Chang, C.-L. "Application of nitrogen-doped graphene nanosheets in electrically conductive adhesives", *Carbon*, **67**, pp. 449-456 (2014).

25. Kumar, M.P., Kesavan, T., Kalita, G., Ragupathy, P., Narayanan, T.N. and Pattanayak, D.K. "On the large capacitance of nitrogen doped graphene derived by a facile route", *RSC Adv.*, **4**(73), pp. 38689-38697 (2014).

26. Aurbach, D., Markovsky, B., Weissman, I., Levi, E. and Ein-Eli, Y. "On the correlation between surface chemistry and performance of graphite negative elec-

trodes for Li ion batteries", *Electrochim. Acta*, **45**(1-2), pp. 67-86 (1999).

27. Beguin, F., Chevallier, F., Vix, C., Saadallah, S., Rouzaud, J.N. and Frackowiak, E. "A better understanding of the irreversible lithium insertion mechanisms in disordered carbons", *J. Phys. Chem. Solids*, **65**(2-3), pp. 211-217 (2004).
28. Verma, P., Maire, P. and Novak, P. "A review of the features and analyses of the solid electrolyte interphase in Li-ion batteries", *Electrochim. Acta*, **55**(22), pp. 6332-6341 (2010).
29. Yan, Z., Liu, L., Guo, H., Tan, J., Shu, H., Yang, X., Hu, H., Zhou, Q., Huang, Z. and Wang, X. "One-pot synthesis of FCNTs-wired TiO_2 nanocomposites as anode materials for high-rate lithium ion batteries", *Electrochim. Acta*, **123**, pp. 551-559 (2014).
30. Lee, S.W., Yabuuchi, N., Gallant, B.M., Chen, S., Kim, B.-S., Hammond, P.T. and Shao-Horn, Y. "High-power lithium batteries from functionalized carbon-nanotube electrodes", *Nat. Nanotechnol.*, **5**(7), pp. 531-537 (2010).
31. Yoo, E., Kim, J., Hosono, E., Zhou, H.-S., Kudo, T. and Honma, I. "Large reversible Li storage of graphene nanosheet families for use in rechargeable lithium ion batteries", *Nano Lett.*, **8**(8), pp. 2277-2282 (2008).
32. Han, X., Chang, C., Yuan, L., Sun, T. and Sun, J. "Aromatic carbonyl derivative polymers as high-performance Li-ion storage materials", *Adv. Mater.*, **19**(12), pp. 1616-1621 (2007).
33. Hu, J., Lu, Q., Tang, K., Yu, S., Qian, Y., Zhou, G. and Liu, X. "Low-Temperature Synthesis of Nanocrystalline Titanium Nitride via a Benzene-Thermal Route", *J. Am. Ceram. Soc.*, **83**(2), pp. 430-32 (2000).
34. Wang, H. and Yoshio, M. "Carbon-coated natural graphite prepared by thermal vapor decomposition process, a candidate anode material for lithium-ion battery", *J. Power Sources*, **93**(1-2), pp. 123-129 (2001).
35. Xiao, X., Liu, P., Wang, J.S., Verbrugge, M.W. and Balogh, M.P. "Vertically aligned graphene electrode for lithium ion battery with high rate capability", *Electrochem. Commun.*, **13**(2), pp. 209-212 (2011).
36. Chen, Y., Song, B., Chen, R.M., Lu, L. and Xue, J. "A study of the superior electrochemical performance of 3 nm SnO_2 nanoparticles supported by graphene", *J. Mater. Chem. A*, **2**(16), pp. 5688-5695 (2014).
37. Pereira, N., Dupont, L., Tarascon, J.M., Klein, L.C. and Amatucci, G.G. "Electrochemistry of Cu_3N with lithium: A complex system with parallel processes", *J. Electrochem. Soc.*, **150**(9), pp. A1273-A1280 (2003).

Biographies

Elahe Yousefi is a PhD Candidate in the Department of Material Science and Engineering at Sharif University of Technology in Tehran, Iran. She received her bachelor (2008) and master (2010) degrees from Tehran Polytechnic and Sharif Universities, respectively. Her research covers a variety of electrochemical problems including synthesis of electrocatalysts, electrodeposition and electrophoretic and respective mechanistic studies, improving anodes performance in Li-ion batteries, fuel cells catalysts and reactions, and their related mechanisms.

Mohammad Ghorbani is a Full Professor at the Department of Material Science and Engineering at Sharif University of Technology in Tehran, Iran. He earned his Master (1986) and Doctoral (1991) degrees from Manchester University, UMIST, UK. His research covers a variety of coatings included in electrodeposition of metallic coatings, composite coatings, conversion coatings, and nano coatings that lead to the publication of more than one hundred ISI papers.

Abolghasem Dolati is a Full Professor at the Department of Material Science and Engineering at Sharif University of Technology in Tehran, Iran. He earned his Master (1995) and Doctoral (2003) degrees from Sharif University of Technology. His research covers a variety of electrochemical issues including electrodeposition of thin films, composites & nanomaterials, kinetics of metals & alloys electrodeposition, modeling & simulation of electrodeposition, and corrosion & protection of materials. In these respects, he has published more than one hundred ISI papers.

Hitoshi Yashiro is a Full Professor at the Department of Chemistry and Bioengineering at Iwate University in Morioka, Japan. He earned his Bachelor (1982) and Doctoral (1994) degrees from Tohoku University. He was an international fellow at SRI International in 1991-1992. His research covers a variety of corrosion problems ranging from lithium ion battery to nuclear power plants. He served as an Editor-in-Chief for Japan Society of Corrosion Engineering in 2009-2011.